Comparision Through Architectures of Semantic Segmentation in Breast Ultrasound Images Across Differents Input Data Dimensions

Clécio Elias Silva E. Silva[a], Salomão Machado Mafalda[b], Emili Silva Bezerra[c], Gustavo Moreira Oliveira de Castro[d], Paulo Chavez dos Santos Júnior[e] and Ana Beatriz Alvarez[f]
PAVIC Laboratory, University of Acre (UFAC), Rio Branco, Acre, Brazil

Keywords: Breast Cancer, Semantic Segmentation, Neural Networks, Deep Learning.

Abstract: Breast cancer is a problem that affects thousands of people every year, early diagnosis is important for the treatment of this disease. Deep learning methods shows impressive results in identification and segmentation of breast cancer task. This paper evaluates the impact of input size images on three semantic segmentation architectures applied to breast tumour ultrasound, in U-net, SegNet and DeepLabV3+. In order to (comprehensively) evaluate each architecture, 5-fold cross validation was carried out, thus reducing the impact of variations in validation and training sets. In addition, the performance of the analyzed architectures was measured using the IoU and Dice metrics. The results showed that the DeepLabV3+ architecture performed better than the others architectures in segmenting breast tumours, achieving an *IoU* of 0.70 and *Dice* of 0.73, with the input dimension of the images being 128×128.

1 INTRODUCTION

Breast cancer is caused by the disorderly proliferation of abnormal cells in the breast that form a tumor that can invade other organs (Doi, 2007). Ultrasound has been one of the most commonly used medical imaging modalities for the assessment of breast masses. It is also more accessible and cheaper than magnetic resonance imaging (Athira et al., 2023).

The evaluation of ultrasound (US) breast images requires extensive knowledge in this field, since this task involves identifying features of malignant and benign breast masses on the images (Gharekhanloo et al., 2018). To assist professionals in interpreting these images, various computer-aided diagnosis (CAD) systems have been developed (Doi, 2007). The segmentation of nodules is of enormous importance in CAD systems, as its correct segmentation allows a more accurate analysis of the morphological features of breast tumors (Jahwar and Abdulazeez, 2022). However, automatic segmentation of US images poses a significant challenge due to the low contrast of US images, the presence of speckle noise, and the considerable variety in sizes and shapes of breast nodules (Gharekhanloo et al., 2018).

Figure 1 illustrates the use of ultrasound images to examine breast nodules. Figure 1.a shows an ultrasound image of a breast with a benign tumor, showing a darker area (highlighted by the green square), with well-defined edges and shape; Figure 1.b shows an image of a breast with a malignant tumor, with a dark spot is highlighted (by the red rectangle), with unclear shape and edges.

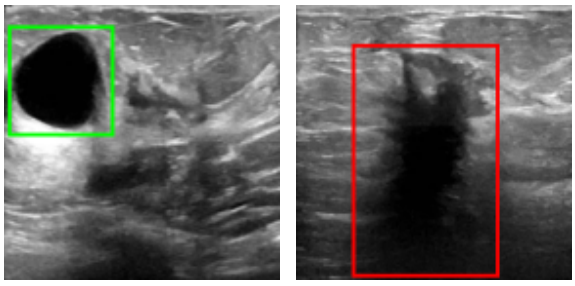

(a) Breast US with benign tumor. (b) Breast US with malignant tumor.

Figure 1: Breast ultrasound images examples.

Accurate segmentation of breast masses in US images involves identification and precise delineation of

[a] https://orcid.org/0009-0000-1599-1167
[b] https://orcid.org/0000-0002-2172-9402
[c] https://orcid.org/0000-0003-4519-8332
[d] https://orcid.org/0009-0002-4014-8803
[e] https://orcid.org/0009-0004-5886-6541
[f] https://orcid.org/0000-0003-3403-8261

Silva, C., Mafalda, S., Bezerra, E., Oliveira de Castro, G., Santos Júnior, P. and Alvarez, A.
Comparision Through Architectures of Semantic Segmentation in Breast Ultrasound Images Across Differents Input Data Dimensions.
DOI: 10.5220/0012322500003657

In *Proceedings of the 17th International Joint Conference on Biomedical Engineering Systems and Technologies (BIOSTEC 2024) - Volume 2*, pages 354-361
ISBN: 978-989-758-688-0; ISSN: 2184-4305

the areas representing the masses, which allows more detailed analysis of their characteristics (Yu et al., 2021). One factor that can directly affect segmentation quality and performance is the resolution of US images, which varies depending on the equipment used. The smaller the pixel size, the better fine details can be captured, which can help in the accurate segmentation of masses (Ploquin et al., 2015). On the other hand, a smaller pixel size can result in a loss of detail and affect the quality of the segmentation.

In addition, the low contrast in US images also represents a challenge for automatic segmentation. The presence of speckle noise in US images can make it difficult to correctly identify breast nodules boundaries. The wide variation in size and shape of breast masses also contributes to the complexity of automatic segmentation in US images (Gokhale, 2009). This diversity requires robust and adaptable algorithms that can handle different scenarios and guarantee reliable results (Ayana et al., 2022).

This paper investigates the influence of input image size on the performance of semantic segmentation neural networks applied to the most commonly used state-of-the-art breast ultrasound images.

By investigating the influence of different input image sizes on the performance of these architectures, the research aims to provide valuable information to optimize the segmentation process of breast ultrasound images, which will ultimately contribute to more accurate and reliable diagnoses of benign and malignant breast cancer nodules.

2 DEEP NEURAL NETWORK ARCHITECTURES

In recent years, several studies have been developed for disease classification, identification, and segmentation in medical images based on deep learning neural networks (Byra et al., 2020; Ayana et al., 2022). Neural networks automatically extract features from images related to some kind of anomaly, unlike classical digital image processing techniques (Sun et al., 2022). The following architectures are most commonly used in the literature: U-net (Ronneberger et al., 2015), DeepLabV3+ (Ayana et al., 2022) and SegNet (Yurtkulu et al., 2019). This paper presents an comparation through these three architectures.

2.1 U-Net

Proposed by (Ronneberger et al., 2015), U-Net is a semantic segmentation neural network architecture originally designed for medical image segmentation tasks such as segmenting blood vessels and brain tumors. U-Net has two main components that gives it the "U" shape: the encoder path to map network inputs to feature map representations by convolutions and max-pooling; and the decoder path to take that feature representation as input using up-convolutions and concatenations that are used for localizing object boundaries. The architecture has 23 convolution layers, as illustrated in Figure 2.

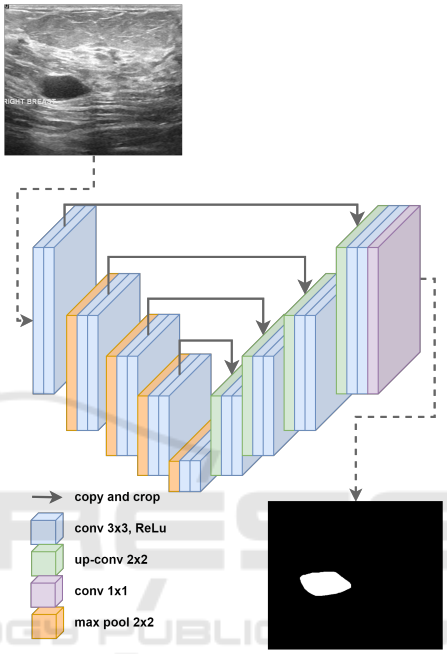

Figure 2: An ilustration of U-Net archtecture. The gray arrows indicate the skip connections that concatenate the encoder feature map with the decoder, which helps the backward flow of gradients for improved training. It consists of a contracting path and an expansive path. The contracting path follows the typical architecture of a convolutional network.

The ability to handle limited amounts of data, robustness to variable image resolutions, and successful application to complex segmentation tasks are features of this architecture (Ronneberger et al., 2015).

2.2 SegNet

The SegNet architecture was proposed by (Badrinarayanan et al., 2017), and is based on the VGG family by the same author with the primary goal of being used in scene understanding applications. With a smaller total number of parameters than other architectures, it has better memory efficiency and speed. Segnet has an encoder-decoder architecture followed by pixel-level classification. The advantage of SegNet is in the way the decoder increases the sampling of its

lower-resolution input feature maps. Specifically, the decoder uses pooling indices computed in the max-pooling phase of the corresponding encoder to perform non-linear upsampling. This eliminates the need to learn how to increase resolution. In this way, high-resolution details are preserved in the segmented image (Badrinarayanan et al., 2017; Cui et al., 2023). The Figure 3 illustrates the SegNet architecture.

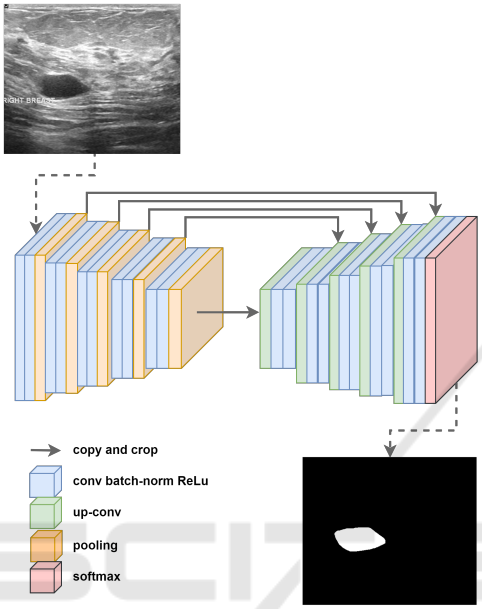

Figure 3: An illustration of the SegNet architecture. There are no fully connected layers and hence it is only convolutional. A decoder upsamples its input using the transferred pool indices from its encoder to produce a sparse feature map(s). It then performs convolution with a trainable filter bank to densify the feature map. The final decoder output feature maps are fed to a soft-max classifier for pixel-wise classification.

2.2.1 DeepLabV3+

The DeepLab family was proposed by Google researchers (Chen et al., 2017). The third version called DeepLabV3 is an encoder-decoder network aimed at performing semantic segmentation tasks. It is capable of capturing multi-contextual information in its encoder by grouping features with multi-rate filtering and pooling operations that expand the receptive field of neurons, while the final layers of the network can capture sharper object boundaries, gradually recovering spatial information. DeeplabV3+ adds a simple but effective decoder module to DeepLabV3, added to improve segmentation results (Liu et al., 2021).

In addition, DeepLabv3+ extends the Atrous Spatial Pyramid Pooling module, which explores convolutional characteristics at various scales, applying atrous convolutions at different rates (Yurtkulu et al., 2019). The Figure 4 illustrates the DeepLabV3+ architecture.

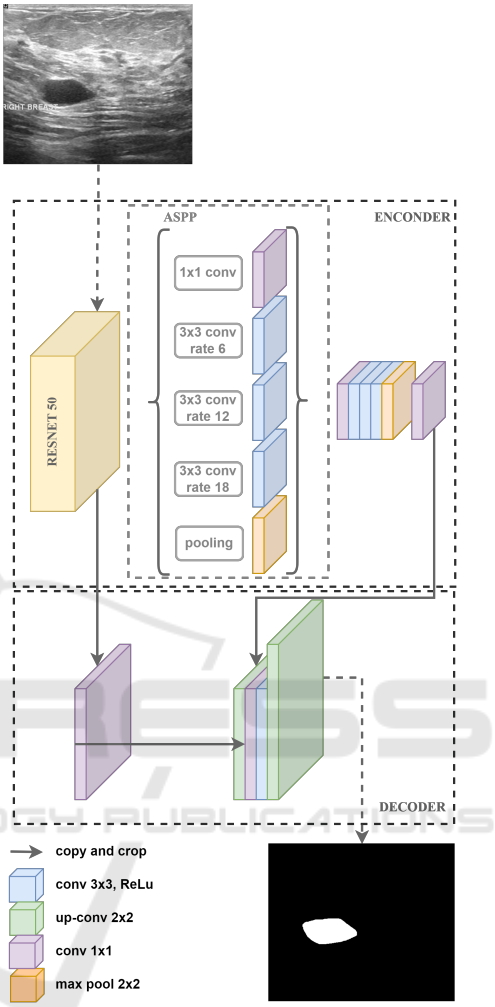

Figure 4: An ilustration of the DeeplabV3+ architecture. The reason for using a Atrous Spatial Pyramid Pooling is that it has been shown that as the sampling rate increases, the number of valid filter weights (i.e., weights applied to the valid feature region instead of padded zeros) becomes smaller (Yurtkulu et al., 2019).

3 MATERIALS AND METHODS

3.1 BUS Dataset

The dataset used is called Breast Ultrasound Images (BUSI) and is made up of breast ultrasound images obtained from ultrasounds of 600 female patients aged between 25 and 75. The BUSI dataset was published in 2018 and has a collection of 780 images,

with average dimensionality of 500x500 pixels. The images were grouped by medical experts into three categories: benign tumor, malignant tumor and normal images. Figure 5 shows examples of images from BUSI dataset. In total, the dataset consists of 437 images of benign tumors and 210 images of malignant tumors and 133 images with no tumors present (Al-Dhabyani et al., 2020). In this article, only the images with tumors present were used.

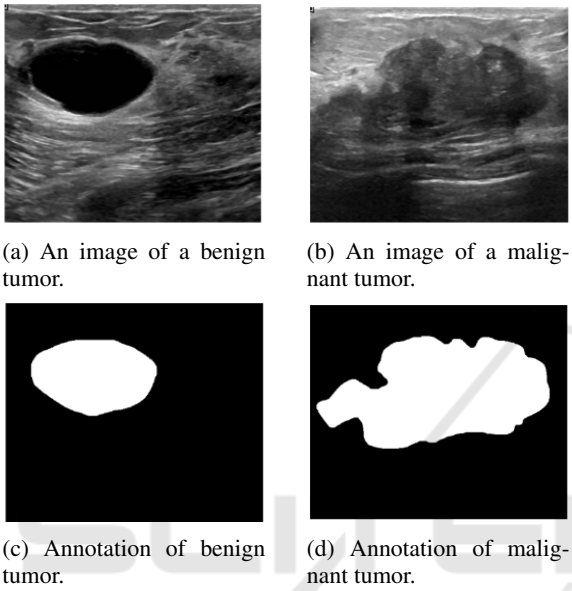

(a) An image of a benign tumor.

(b) An image of a malignant tumor.

(c) Annotation of benign tumor.

(d) Annotation of malignant tumor.

Figure 5: Examples of breast ultrasound images from the Dataset and their respective annotations.

3.2 Data Pre-Processing

For the neural networks semantic segmentation training, the annotations made by the experts were merged into a single mask. Figure 6 shows the process for merging 3 annotations of the tumors to form a single output image.

In addition, in order to assess the dimensionality impact of the input data on the segmentation performance, five sets of data were created for training, differing only in the size of the images. The dimensions established and analyzed in this article were: 32×32, 64×64, 128×128, 256×256 and 512×512. Finally, the data was divided into training, validation and testing sets, following the proportion of 80%, 10% and 10% respectively.

Images of the malignant tumor class were augmented to balance the dataset. The techniques used were Horizontal Flip, Vertical Flip, Rotation 90º and Transpose. 437 images were obtained for both the malignant and benign classes, as shown in Figure 7.

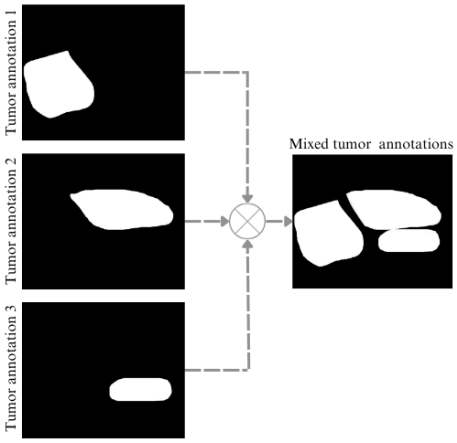

Figure 6: Illustration of the annotation merging process.

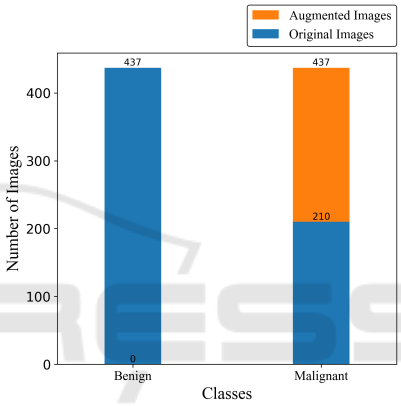

Figure 7: Illustration graphically representing the total number of images.

3.3 Deep Neural Network Training

The dimensionality of the data varies in different proportions, from 32 to 512, and the architectures remain with the same number of layers in all experiments. For this reason, the regularization technique called Early Stopping was used to avoid overffiting. This method looks at the performance of the training data and the validation set, this way when the model is fitting the training data and making errors in the validation data, i.e. not generalizing, the method defines early stopping rules before the model starts to overfit. This article used Early Stopping with a patience of 20, i.e. the model was evaluated with the weights 20 epochs after overfitting.

The other hyperparameters used to train the architectures are shown in Table 1.

To illustrate the training process, Figure 8 shows the loss and learning curve of the Segnet model for the 64×64 dimension. A maximum of 100 epochs was used for all training.

Table 1: Hyperparameter table applied to training.

Hyperparameter	Value
Learning rate	0.001
Batch-size	32
Epochs	100
Patience	20
Optimizer	Adam

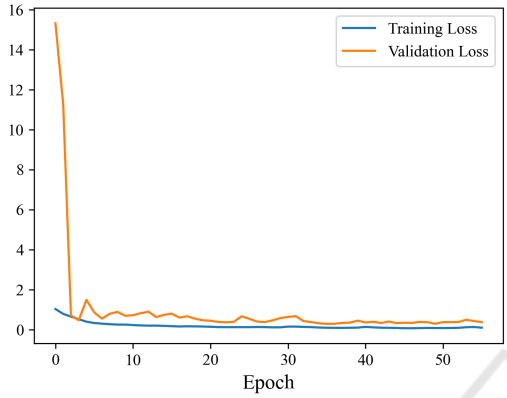

(a) Training and validation loss curve.

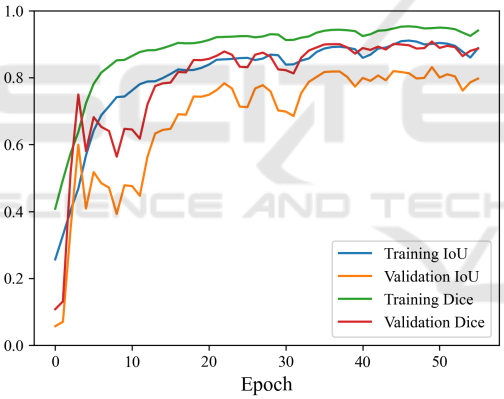

(b) Training and validation metrics.

Figure 8: Comparison of loss curve and metrics for training and validation.

A K-Fold cross-validation ($K = 5$) was carried out. This means that the data set was randomly divided into five distinct parts, and the models were trained and validated five times, alternating the training and validation parts in each iteration. This procedure helps to evaluate the model's performance more comprehensively, reducing the impact of variations in the training and validation sets and providing a reliable estimation of its ability to generalize (Bishop and Nasrabadi, 2006).

For the results, the average of the performance metrics obtained from cross-validation for each method and input image size and class was calculated. The differences in the results of the 5-Folds, for the same input image size, showed an overall average of approximately 0.06.

The low variance indicates that the models perform similarly in all parts of the dataset during the cross-validation process, as proven by (Ostertagova et al., 2014). Therefore, the results obtained in any of the trained models can be considered representative for all of them, providing a stable assessment of their ability to generalize.

4 RESULTS AND DISCUSSION

This section presents the results obtained for the experiments carried out for the three architectures evaluated: U-Net, SegNet and DeepLabV3+.

4.1 U-Net

Table 2 shows the results of the tests carried out with the U-net architecture. The first column shows the input image sizes, the second column refers to the segmented classes, while the last two columns show the IoU and Dice. IoU and Dice for the benign tumor class varies between $0.57 - 0.65$ and $0.60 - 0.67$ with a standard deviation between $0.32 - 0.42$ and $0.34 - 0.40$, respectively. For the malignant tumor class, IoU and Dice varies between $0.31 - 0.56$ and $0.35 - 0.60$ with a standard deviation between $0.32 - 0.40$ and $0.34 - 0.37$, respectively.

Superior performance can be seen when the model's input image dimension is set to 64×64. With IoU of 0.65 and Dice of 0.67 for the benign tumor class and IoU of 0.56 and Dice of 0.60 for the malignant tumor class. Obtaining an average for both classes of 0.60 for IoU and 0.64 for Dice.

Table 2: Segmentation performance scores (and standard deviation) achieved by U-Net for different input image sizes.

Size	Class	IoU	Dice
32×32	Benign	0.65±0.38	0.67±0.36
	Malignant	0.53±0.36	0.57±0.36
64×64	**Benign**	**0.65±0.37**	**0.67±0.38**
	Malignant	**0.56±0.35**	**0.60±0.35**
128 × 128	Benign	0.63±0.40	0.65±0.40
	Malignant	0.52±0.36	0.56±0.37
256 × 256	Benign	0.62±0.41	0.64±0.41
	Malignant	0.39±0.40	0.44±0.37
512 × 512	Benign	0.57±0.42	0.60±0.42
	Malignant	0.31±0.32	0.35±0.34

Table 3: Segmentation performance scores (and standard deviation) achieved by SegNet for different input image sizes.

Size	Class	IoU	Dice
32×32	Benign	0.59±0.42	0.60±0.45
	Malignant	0.46±0.43	0.51±0.43
64×64	Benign	0.59±0.41	0.61±0.40
	Malignant	0.57±0.38	0.61±0.38
128×128	Benign	0.61±0.39	0.64±0.39
	Malignant	0.59±0.37	0.62±0.37
256×256	**Benign**	**0.66±0.39**	**0.69±0.39**
	Malignant	**0.59±0.38**	**0.63±0.38**
512×512	Benign	0.65±0.38	0.68±0.39
	Malignant	0.42±0.37	0.46±0.38

Table 4: Segmentation performance scores (and standard deviation) achieved by DeeplabV3+ for different input image sizes.

Size	Class	IoU	Dice
32×32	Benign	0.69±0.36	0.73±0.35
	Malignant	0.54±0.36	0.61±0.36
64×64	Benign	0.68±0.38	0.71±0.38
	Malignant	0.60±0.39	0.63±0.38
128×128	**Benign**	**0.77±0.33**	**0.79±0.33**
	Malignant	**0.63±0.35**	**0.66±0.35**
256×256	Benign	0.73±0.37	0.74±0.37
	Malignant	0.59±0.39	0.61±0.39
512×512	Benign	0.68±0.40	0.69±0.40
	Malignant	0.51±0.40	0.53±0.40

4.2 SegNet

Table 3 shows the results of the tests carried out with the SegNet architecture. The first column shows the input image sizes, the second column refers to the segmented classes, while the last two columns show the IoU and Dice. IoU and Dice for the benign tumor class varies between $0.59 - 0.66$ and $0.60 - 0.69$ with a standard deviation between $0.38 - 0.42$ and $0.39 - 0.45$, respectively. For the malignant tumor class, IoU and Dice varies between $0.42 - 0.59$ and $0.46 - 0.63$ with a standard deviation between $0.37 - 0.43$ and $0.37 - 0.43$, respectively.

The Table 3 shows that the results obtained are similar to those of U-Net. The standard deviation for both benign and malignant classes was between 0.37 and 0.44 for IoU and 0.37 and 0.45 for Dice.

The architecture performed best in the 256×256 dimension. With IoU of 0.66 and Dice of 0.69 for the benign and IoU of 0.59 and Dice of 0.63 for malignant tumor class. The average IoU and Dice were 0.63 and 0.66, respectively.

4.3 DeepLabV3+

Table 4 shows the results of the tests carried out with the DeepLabV3+ architecture. The first column shows the input image sizes, the second column refers to the segmented classes, while the last two columns show the IoU and Dice. IoU and Dice for the benign tumor class varies between $0.68 - 0.77$ and $0.69 - 0.79$ with a standard deviation between $0.33 - 0.40$ for both metrics. For the malignant tumor class, IoU and Dice varies between $0.51 - 0.63$ and $0.53 - 0.66$ with a standard deviation between $0.35 - 0.40$ for both metrics.

The architecture performed best in the 128×128 dimension. With average IoU and Dice of 0.70 and 0.73, respectively.

4.4 Comparison Through Architectures

When comparing the three architectures implemented, we can see a good performance in all architectures. U-net achieved the best performance with an input size of 64×64, as shown in section 4.1. SegNet achieved better performance with an input size of 256×256, as presented in section 4.2, with averages of 0.60 for IoU and 0.64 for Dice. DeepLabV3+ performed best with an input size of 128×128, as shown in section 4.3, with averages of 0.63 and 0.66 for IoU and Dice, respectively. The results obtained for the DeepLabV3+ architecture were superior in all dimensions tested for the other architectures, as shown in Table 5, with an average of 0.70 and 0.73 for IoU and Dice, respectively.

To illustrate the implementation of the three analyzed architectures, Figure 9 shows an example created for U-net, SegNet, and DeepLabV3+. The first column shows the original image, the second column shows the ground truth, and the third column the prediction of the architecture. The figure shows a small tumor with poorly defined edges. In the figure, it can be seen that DeepLabV3+ correctly segmented the benign tumor (in orange), while SegNet misclassified the tumor, i.e., predicted it as a malignant tumor (green) even though it was benign (orange). U-Net's prediction was inferior to the other two architectures because it predicted two classes simultaneously. For tumors with large proportions and well-defined edges, an example has been created and is shown in Figure 10. It can be seen that DeepLabV3+ and U-Net correctly segmented the benign tumor (in orange), while SegNet prediction was inferior to the other two architectures because it predicted two classes simultaneously.

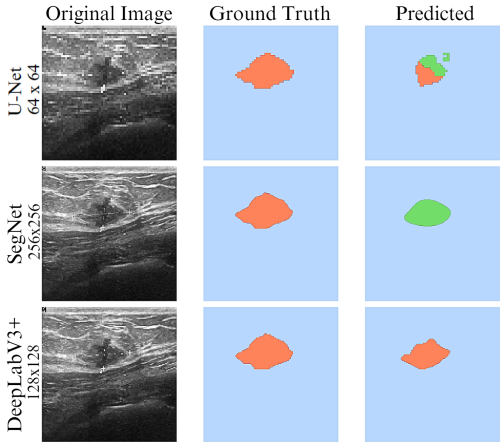

Figure 9: Example of tumor segmentation with small tumor with poorly defined edges at different image sizes on the analyzed architectures.

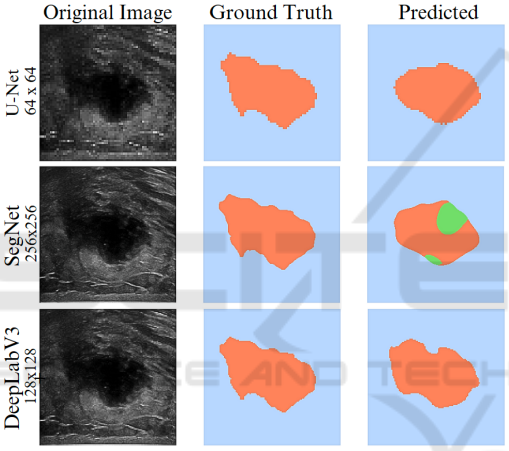

Figure 10: Example of tumor segmentation with large proportions and well-defined edges at different image sizes on the analyzed architectures.

5 CONCLUSION

In this paper was evaluated the impact of the image input size on semantic segmentation models applied to breast tumor ultrasound, where the architectures selected were U-net, SegNet and DeepLabV3+. The architectures were evaluated using IoU and Dice. In addition, to check the generalization capability of segmentation architectures models was used independent training-test experiments based on the k-fold cross-validation method.

It was observed that the three architectures tested performed differently in terms of image dimensions. The U-net, Segnet and DeepLabV3+ architectures performed best with input dimensions of 64×64, 256×256 and 128×128, respectively. These findings indicate that the sizing of input images is a critical factor in obtaining accurate and reliable results in breast tumors segmentation. Each model showed different preferences in relation to dimension, which highlights the importance of a careful analysis of the specific characteristics of each method when applying them to different clinical and research contexts.

Table 5: Segmentation performance scores achieved by the three architectures.

Size	Architectures	IoU	Dice
32×32	U-net	0.59	0.62
	SegNet	0.54	0.56
	DeepLabV3+	**0.62**	**0.67**
64×64	U-net	0.60	0.64
	SegNet	0.58	0.61
	DeepLabV3+	**0.64**	**0.67**
128×128	U-net	0.57	0.61
	SegNet	0.60	0.63
	DeepLabV3+	**0.70**	**0.73**
256×256	U-net	0.50	0.54
	SegNet	0.63	0.66
	DeepLabV3+	**0.66**	**0.68**
512×512	U-net	0.44	0.47
	SegNet	0.54	0.57
	DeepLabV3+	**0.59**	**0.61**

Furthermore, the significant variation in IoU and Dice results for different tumor classes emphasizes the need to consider the peculiarities of each tumor type when choosing the appropriate image dimension for segmentation. This detailed understanding can optimize the accuracy of the segmentation process and, consequently, improve the detection and follow-up of breast tumors.

According to the results, DeepLabV3+, among all the architectures analyzed, obtained the best performance in semantic segmentation of breast tumors. As expected, segmentation performance improves as network depth increases. This behavior happens because deeper networks extracted more subtle features that distinguish normal and abnormal patterns in breast tissue, while shallower networks extracted global image features.

For approximately two decades, researchers developed CAD systems with high generalization capability that are useful in clinical practice. A comparison of the different data input dimensions revealed their potential to increase breast screening efficiency and effectiveness. Hence, the experimental results encourage the use of DeepLabV3+ model within a CAD system for the automated segmentation of breast tumors.

Therefore, the appropriate choice of dimension is a fundamental role in the effectiveness and accuracy

of the predictions of semantic segmentation models. This information is valuable for guiding future research and clinical applications aimed at improving the diagnosis and treatment of this important cancer pathology.

ACKNOWLEDGEMENTS

The work presented in this paper was supported by the *Pesquisa Aplicada em Visão e Inteligência Computacional* (PAVIC) project at Universidade Federal do Acre, Brazil.

REFERENCES

Al-Dhabyani, W., Gomaa, M., Khaled, H., and Fahmy, A. (2020). Dataset of breast ultrasound images. *Data in brief*, 28:104863.

Athira, K., Dharmarajan, J. P., Vijaykumar, D., and Subbanna, N. (2023). Analysis of the various techniques used for breast segmentation from mammograms. In *2023 International Conference on Distributed Computing and Electrical Circuits and Electronics (ICDCECE)*, pages 1–7. IEEE.

Ayana, G., Dese, K., Raj, H., Krishnamoorthy, J., and Kwa, T. (2022). De-speckling breast cancer ultrasound images using a rotationally invariant block matching based non-local means (ribm-nlm) method. *Diagnostics*, 12(4):862.

Badrinarayanan, V., Kendall, A., and Cipolla, R. (2017). Segnet: A deep convolutional encoder-decoder architecture for image segmentation. *IEEE transactions on pattern analysis and machine intelligence*, 39(12):2481–2495.

Bishop, C. M. and Nasrabadi, N. M. (2006). *Pattern recognition and machine learning*, volume 4. Springer.

Byra, M., Jarosik, P., Szubert, A., Galperin, M., Ojeda-Fournier, H., Olson, L., O'Boyle, M., Comstock, C., and Andre, M. (2020). Breast mass segmentation in ultrasound with selective kernel u-net convolutional neural network. *Biomedical Signal Processing and Control*, 61:102027.

Chen, L.-C., Papandreou, G., Kokkinos, I., Murphy, K., and Yuille, A. L. (2017). Deeplab: Semantic image segmentation with deep convolutional nets, atrous convolution, and fully connected crfs. *IEEE transactions on pattern analysis and machine intelligence*, 40(4):834–848.

Cui, W., Meng, D., Lu, K., Wu, Y., Pan, Z., Li, X., and Sun, S. (2023). Automatic segmentation of ultrasound images using segnet and local nakagami distribution fitting model. *Biomedical Signal Processing and Control*, 81:104431.

Doi, K. (2007). Computer-aided diagnosis in medical imaging: historical review, current status and future potential. *Computerized medical imaging and graphics*, 31(4-5):198–211.

Gharekhanloo, F., Haseli, M. M., and Torabian, S. (2018). Value of ultrasound in the detection of benign and malignant breast diseases: a diagnostic accuracy study. *Oman Medical Journal*, 33(5):380.

Gokhale, S. (2009). Ultrasound characterization of breast masses. *Indian Journal of Radiology and Imaging*, 19(03):242–247.

Jahwar, A. F. and Abdulazeez, A. M. (2022). Segmentation and classification for breast cancer ultrasound images using deep learning techniques: a review. In *2022 IEEE 18th International Colloquium on Signal Processing & Applications (CSPA)*, pages 225–230. IEEE.

Liu, M., Fu, B., Xie, S., He, H., Lan, F., Li, Y., Lou, P., and Fan, D. (2021). Comparison of multi-source satellite images for classifying marsh vegetation using deeplabv3 plus deep learning algorithm. *Ecological Indicators*, 125:107562.

Ostertagova, E., Ostertag, O., and Kováč, J. (2014). Methodology and application of the kruskal-wallis test. *Applied mechanics and materials*, 611:115–120.

Ploquin, M., Basarab, A., and Kouame, D. (2015). Resolution enhancement in medical ultrasound imaging. *Journal of Medical Imaging*, 2(1):171.

Ronneberger, O., Fischer, P., and Brox, T. (2015). U-net: Convolutional networks for biomedical image segmentation. In *Medical Image Computing and Computer-Assisted Intervention–MICCAI 2015: 18th International Conference, Munich, Germany, October 5-9, 2015, Proceedings, Part III 18*, pages 234–241. Springer.

Sun, Y., Yang, H., Zhou, J., and Wang, Y. (2022). Issmf: Integrated semantic and spatial information of multi-level features for automatic segmentation in prenatal ultrasound images. *Artificial Intelligence in Medicine*, 125:102254.

Yu, K., Chen, S., and Chen, Y. (2021). Tumor segmentation in breast ultrasound image by means of res path combined with dense connection neural network. *Diagnostics*, 11(9):1565.

Yurtkulu, S. C., Şahin, Y. H., and Unal, G. (2019). Semantic segmentation with extended deeplabv3 architecture. In *2019 27th Signal Processing and Communications Applications Conference (SIU)*, pages 1–4. IEEE.